J Braz. Soc. Mech. Sci. Eng. (2016) 38:85–98
DOI 10.1007/s40430-015-0389-2

TECHNICAL PAPER

Unaxisymmetric stagnation-point flow and heat transfer of a viscous fluid on a moving cylinder with time-dependent axial velocity

Rasool Alizadeh[1] · Asghar B. Rahimi[2] · Mohammad Najafi[1]

Received: 14 December 2014 / Accepted: 20 June 2015 / Published online: 28 July 2015

Abstract The unsteady viscous flow and heat transfer in the vicinity of an unaxisymmetric stagnation-point flow of an infinite moving cylinder with time-dependent axial velocity and non-uniform normal transpiration $U_0(\varphi)$ are investigated. The impinging free stream is steady with a strain rate $\bar{k}$. A reduction of the Navier–Stokes and energy equations is obtained by use of appropriate similarity transformations. The semi-similar solution of the Navier–Stokes equations and energy equation has been obtained numerically using an implicit finite-difference scheme when the axial velocity of the cylinder and its wall temperature or its wall heat flux varies as specified time-dependent functions. In particular, the cylinder may move with different velocity patterns. These solutions are presented for special cases when the time-dependent axial velocity of the cylinder is a step function, a ramp, and a non-linear function. All the solutions above are presented for Reynolds numbers, $\mathrm{Re} = \bar{k}a^2/2\upsilon$, ranging from 0.1 to 100 for different values of Prandtl number and for selected values of transpiration rate function, $S(\varphi) = U_0(\varphi)/\bar{k}a$ where a is cylinder radius and υ is kinematic viscosity of the fluid. Dimensionless shear stresses corresponding to all the cases increase with the increase of Reynolds number and transpiration rate function. An interesting result is obtained in which a cylinder moving with certain axial velocity function and at particular value of Reynolds number is axially stress free. The heat transfer coefficient increases with the increasing transpiration rate function, Reynolds number and Prandtl number. Interesting means of cooling and heating processes of cylinder surface are obtained using different rates of transpiration rate function. It is shown that a cylinder with certain type of exponential wall temperature exposed to a temperature difference has not heat transfer.

Keywords Unaxisymmetric stagnation flow · Axial movement · Non-uniform transpiration

List of symbols

a	Cylinder radius
r	Radial coordinate
z	Axial coordinate
u, w	Velocity components along (r, z)-axis
t	Time
T	Temperature
T_W	Wall temperature
T_∞	Free-stream temperature
k	Thermal conductivity
$\bar{k}$	Free-stream strain rate
$f(\eta,\ \varphi,\ \tau)$	Function related to u-component of velocity
$H(\eta,\ \varphi,\ \tau)$	Function related to w-component of velocity
$V(t)$	Axial velocity of cylinder
$U_0(\varphi)$	Transpiration
Re	Reynolds number
Pr	Prandtl number
Nu	Nusselt number
$S(\varphi)$	Transpiration rate function

Technical Editor: Francisco Ricardo Cunha.

✉ Asghar B. Rahimi
rahimiab@yahoo.com

Rasool Alizadeh
R_alizadeh86@yahoo.com

Mohammad Najafi
M.njafi36@gmail.com

[1] Department of Mechanical and Aerospace Engineering, Tehran Science and Research Branch, Islamic Azad University, Tehran, Iran

[2] Faculty of Engineering, Ferdowsi University of Mashhad, P.O. Box No. 91775-1111, Mashhad, Iran

P	Non-dimensional fluid pressure
p	Fluid pressure
h	Heat transfer coefficient
q_w	Heat flux at wall

Greek symbols

η	Similarity variable
φ	Angular coordinate
α	Thermal diffusivity
ρ	Fluid density
υ	Kinematic viscosity
μ	Dynamic viscosity
$\theta(\eta, \varphi, \tau)$	Non-dimensional temperature
σ	Shear stress
τ	Dimensionless time variable

1 Introduction

There are many solutions of the Navier–Stockes and energy Equations regarding the problem of stagnation-point flow and heat transfer in the vicinity of a flat plate or a cylinder. These studies started by Hiemenz [1], who obtained an exact solution of the Navier–Stokes equations governing the two-dimensional stagnation-point flow on a flat plate, and were continued by Homann [2] with an analogous axisymmetric study and by Howarth [3] and Davey [4], whose results for stagnation flow against a flat plate for asymmetric cases were presented. Wang [5, 6] was the first to find an exact solution for the problem of axisymmetric stagnation-point flow on an infinite stationary circular cylinder; this was continued by Gorla's [7–11] works, which are a series of steady and unsteady flows and heat transfer over a circular cylinder in the vicinity of the stagnation-point for the cases of constant axial movement and the special case of axial harmonic motion of a non-rotating cylinder. Cunning et al. [12] have considered the stagnation-point flow problem on a rotating circular cylinder with constant angular velocity; Grosch and Salwen [13] as well as Takhar et al. [14] studied special cases of unsteady viscous flow on an infinite circular cylinder. The most recent works of the same types are the ones by Saleh and Rahimi [15] and Rahimi and Saleh [16, 17], which are exact solution studies of a stagnation-point flow and heat transfer on a circular cylinder with time-dependent axial and rotational movements, as well as studies by Abbasi and Rahimi [18–21], which are exact solutions of stagnation-point flow and heat transfer but on a flat plate. Some existing compressible flow studies but in the stagnation-point region of bodies and using boundary layer equations include the study by Subhashini and Nath [22] as well as Kumari and Nath[23, 24], which are in the stagnation region of a body, and work of Katz [25] as well as Afzal and Ahmad [26], Libby [27], and Gersten et al. [28], which are all general studies in the stagnation region of a body.

The effects of cylinder movement with time-dependent axial velocity and non-uniform normal transpiration in general, especially with different types of harmonic oscillation, which are of interest in certain special manufacturing processes, textile technology, Printing Industry, water show technology, cooling and centrifugal processes in industry, calcinations of cement and accelerating phases of rocket motors, have not yet been considered. Our motivation is originally to produce friction-less situations in fluids and insulated surfaces in heat transfer by means of certain types of movements and temperature difference. Since the decay of viscosity in a fluid and diffusion of heat in a medium is naturally exponential, selection of the corresponding function in this study serves appropriate examples. Besides, our study generalizes the problem of stagnation-point flow and heat transfer of a fluid on a moving cylinder.

All the studies mentioned above are regarding the axisymmetric flow and heat transfer and none has considered the effect of flow being unaxisymmetric. In the present analysis, the problem of unsteady viscous flow and heat transfer in the vicinity of an unaxisymmetric stagnation-point flow of an infinite cylinder with time-dependent axial movement and non-uniform normal transpiration is considered for the first time. A reduction of the Navier–Stokes and energy equations is obtained by use of appropriate similarity transformations. The semi-similar solution of these equations is obtained numerically using an implicit finite-difference scheme when the axial velocity of the cylinder and its wall temperature or its wall heat flux varies as specified time-dependent functions. In particular, the cylinder may move with different velocity patterns. These solutions are presented for special cases when the time-dependent axial velocity of the cylinder is a step function, a ramp, and a non-linear function All the solutions above are presented for Reynolds numbers, $\mathrm{Re} = \bar{k}a^2/2\upsilon$, ranging from 0.1 to 100 for different values of Prandtl number and for selected values of transpiration rate function, $S(\varphi) = U_0(\varphi)/\bar{k}a$ where a is cylinder radius and υ is kinematic viscosity of the fluid. Dimensionless shear stresses corresponding to all the cases increase with the increase of Reynolds number and transpiration rate function. An interesting result is obtained in which a cylinder moving with certain axial velocity function and at particular value of Reynolds number is axially stress free. The heat transfer coefficient increases with the increasing transpiration rate function, Reynolds number and Prandtl number. Interesting means of cooling and heating processes of cylinder surface are obtained using different rates of transpiration. It is shown that a cylinder with certain type of exponential wall temperature exposed to a temperature difference has not heat transfer.

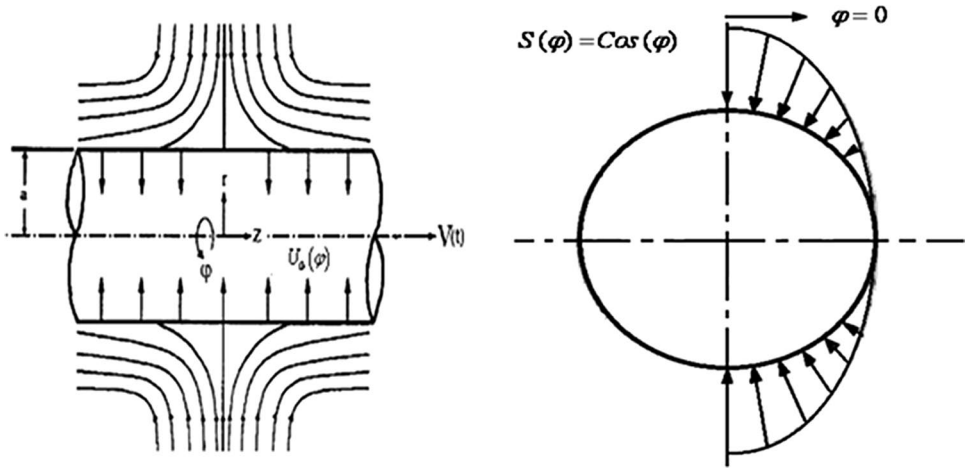

Fig. 1 Schematic diagram of an axially moving cylinder under radial stagnation flow

2 Problem formulation

Flow is considered in cylindrical coordinates $(r,\ \varphi,\ z)$ with corresponding velocity components $(u,\ v,\ w)$; see Fig. 1. An external axisymmetric radial stagnation-point flow of strain rate $\bar{k}$ impinges on the cylinder of radius a, centered at $r = 0$. Because of existence of a selected transpiration function shown below, a laminar unsteady incompressible flow and heat transfer of a viscous fluid in the neighborhood of an unaxisymmetric stagnation-point of an infinite circular cylinder when it moves axially with a velocity that varies with time forms.

The unsteady Navier–Stokes and energy equations in cylindrical polar coordinates governing the unaxisymmetric incompressible flow and heat transfer are as follows:

Mass:

$$\frac{\partial u}{\partial r}+\frac{u}{r}+\frac{\partial w}{\partial z}=0 \tag{1}$$

r-Momentum:

$$\frac{\partial u}{\partial t}+u\frac{\partial u}{\partial r}+w\frac{\partial u}{\partial z} =-\frac{1}{\rho}\frac{\partial p}{\partial r}+\upsilon\left[\frac{\partial^2 u}{\partial r^2}+\frac{1}{r}\frac{\partial u}{\partial r}-\frac{u}{r^2}+\frac{1}{r^2}\frac{\partial^2 u}{\partial \varphi^2}+\frac{\partial^2 u}{\partial z^2}\right] \tag{2}$$

z-Momentum:

$$\frac{\partial w}{\partial t}+u\frac{\partial w}{\partial r}+w\frac{\partial w}{\partial z} =-\frac{1}{\rho}\frac{\partial p}{\partial z}+\upsilon\left[\frac{\partial^2 w}{\partial r^2}+\frac{1}{r}\frac{\partial w}{\partial r}+\frac{1}{r^2}\frac{\partial^2 w}{\partial \varphi^2}+\frac{\partial^2 w}{\partial z^2}\right] \tag{3}$$

Energy:

$$\frac{\partial T}{\partial t}+u\frac{\partial T}{\partial r}+w\frac{\partial T}{\partial z}=\alpha\left[\frac{\partial^2 T}{\partial r^2}+\frac{1}{r}\frac{\partial T}{\partial r}+\frac{1}{r^2}\frac{\partial^2 T}{\partial \varphi^2}+\frac{\partial^2 T}{\partial z^2}\right] \tag{4}$$

where p, ρ, υ and T are the fluid pressure, density, kinematic viscosity, and temperature inside the boundary layer and after the impingement has occurred, respectively. The boundary conditions for the velocity field are:

$$r=a: \qquad u=-U_0(\varphi) \qquad w=a\cdot V(t) \tag{5}$$

$$r\to\infty: \qquad \frac{\partial u}{\partial r}=-\bar{k}, \qquad w=2\bar{k}z \tag{6}$$

And the two boundary conditions with respect to φ are:

$$u(r,\ 0,\ t)=u(r,\ 2\pi,\ t)$$
$$\frac{\partial u(r,\ 0,\ t)}{\partial \varphi}=\frac{\partial u(r,\ 2\pi,\ t)}{\partial \varphi} \tag{7}$$

In which Eq. (5) represents no-slip conditions on the cylinder wall, and the relations of Eq. (6) show that the viscous flow solution approaches, in a manner analogous to the Hiemenz flow, the potential flow solution as $r\to\infty$. This can be confirmed by starting from continuity equation as the following:

$-\frac{1}{r}\frac{\partial}{\partial r}(ru)=\frac{\partial w}{\partial z}=$ Constant and $=2\bar{k}z$ integrating in r and z directions with boundary conditions: $w=0$ when $z=0$ and $u=-U_0(\varphi)$ when $r=a$

For the temperature field, we have

$r=a$: (i) $T=T_{\mathrm{w}}(t)$ for defined wall temperature

(ii) $\dfrac{\partial T}{\partial r}=-\dfrac{q_{\mathrm{w}}(t)}{k}$ for defined wall heat flux

$$r\to\infty: \qquad T\to T_\infty \tag{8}$$

And the two boundary conditions with respect to φ are

$$T(r,0,\tau)=T(r,2\pi,\tau)$$
$$\frac{\partial T(r,0,\tau)}{\partial \varphi}=\frac{\partial T(r,2\pi,\tau)}{\partial \varphi} \tag{9}$$

where k is the thermal conductivity of the fluid and $T_{\mathrm{w}}(t)$ and $q_{\mathrm{w}}(t)$ are temperature and heat flux at the wall cylinder,

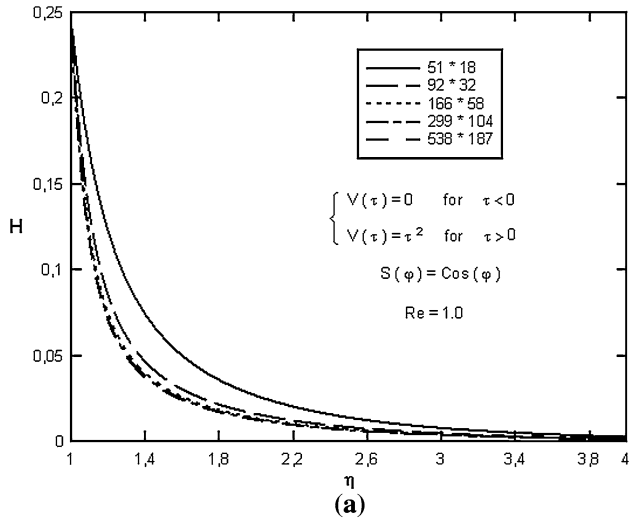

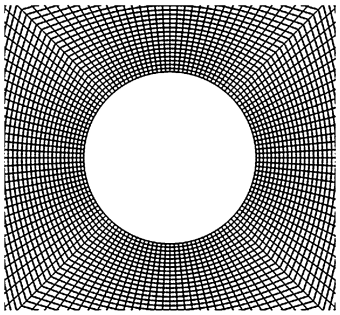

Fig. 2 **a** Sample profiles of $H(\eta,\ \varphi,\ \tau)$ distributions on the cylinder for various mesh sizes at Re = 1.0, $S(\varphi) = Cos(\varphi)$ and axial velocity functions $V(\tau) = \tau^2$. **b** Sample of grid system

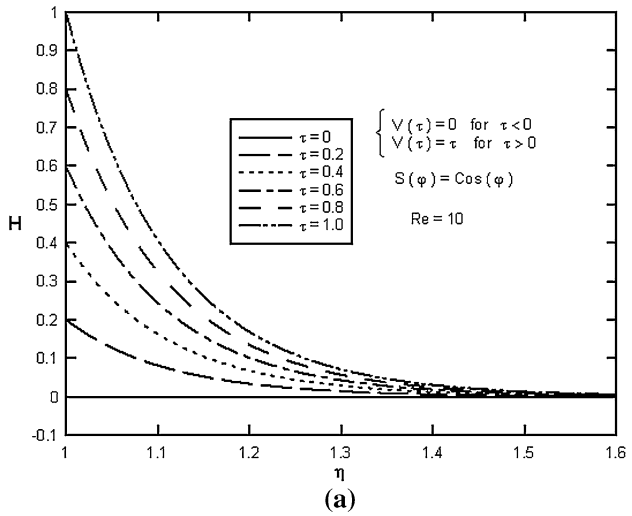

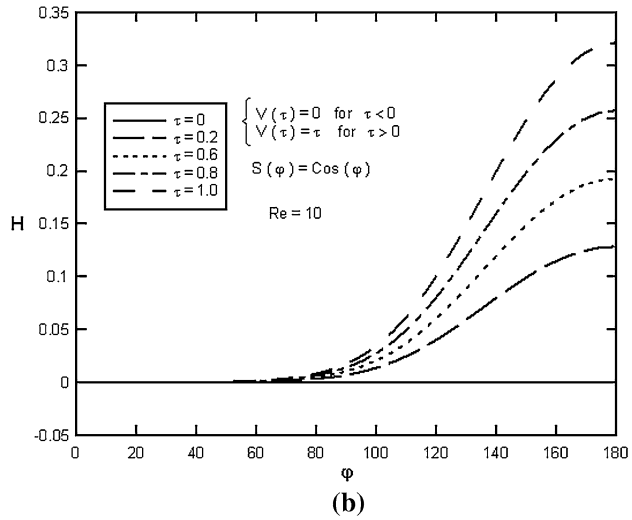

Fig. 3 Sample profiles of $H(\eta,\ \varphi,\ \tau)$ for axial velocity functions $V(\tau) = \tau$ in terms of **a** η, **b** φ at Re = 10, $S(\varphi) = Cos(\varphi)$ and for selected values of time steps

respectively, and T_∞ is the free stream temperature. A reduction of the Navier–Stokes equations is obtained by applying the following transformations:

$$u = -\frac{\bar{k}a}{\sqrt{\eta}} f(\eta,\ \varphi,\ \tau),$$
$$w = 2\bar{k} f'(\eta,\ \varphi,\ \tau)z + H(\eta,\ \varphi,\ \tau) \tag{10}$$

$$\eta = \left(\frac{r}{a}\right)^2, \quad \tau = 2\bar{k}t, \quad p = \rho\bar{k}^2 a^2 P$$

where $\tau = 2\bar{k}t$ and $\eta = \left(\frac{r}{a}\right)^2$ is dimensionless time and radial variable and prime denotes differentiation with respect to η. Transformations (10) satisfy Eq. (1) automatically and their insertion into Eq. (2) and (3) yields a coupled system of differential equations in terms of $f(\eta,\ \varphi,\ \tau)$ and $H(\eta,\ \varphi,\ \tau)$ and an expression for the pressure:

$$P - P_0 = -\frac{1}{2}\left(\frac{f^2}{\eta}\right) - \left(\frac{f'}{\mathrm{Re}}\right) - \frac{1}{4\mathrm{Re}}\int_1^\eta \frac{1}{\eta^2}\frac{\partial^2 f}{\partial\varphi^2}\mathrm{d}\eta - 2\left(\frac{z}{a}\right)^2 \tag{11}$$

$$\eta f''' + f'' + \frac{1}{4\eta}\frac{\partial^2 f'}{\partial\varphi^2} + \mathrm{Re}\left[1 + ff'' - (f')^2 - \frac{\partial f'}{\partial\tau}\right] = 0 \tag{12}$$

$$\eta H'' + H' + \frac{1}{4\eta}\frac{\partial^2 H}{\partial\varphi^2} + \mathrm{Re}\left[fH' - f'H - \frac{\partial H}{\partial\tau}\right] = 0 \tag{13}$$

In these equations, $\mathrm{Re} = \bar{k}a^2/2\upsilon$ is the Reynolds number and prime indicates differentiation with respect to η. From conditions (5), (6) and (7), the boundary conditions for Equations (12) and (13) are as follows:

$$\eta = 1: \quad f(1,\ \varphi,\ \tau) = S(\varphi), \quad f'(1,\ \varphi,\ \tau) = 0,$$
$$H(1,\ \varphi,\ \tau) = V(\tau) \tag{14}$$

$$\eta \to \infty: \quad f'(\infty,\ \varphi,\ \tau) = 1, \quad H(\infty,\ \varphi,\ \tau) = 0 \tag{15}$$

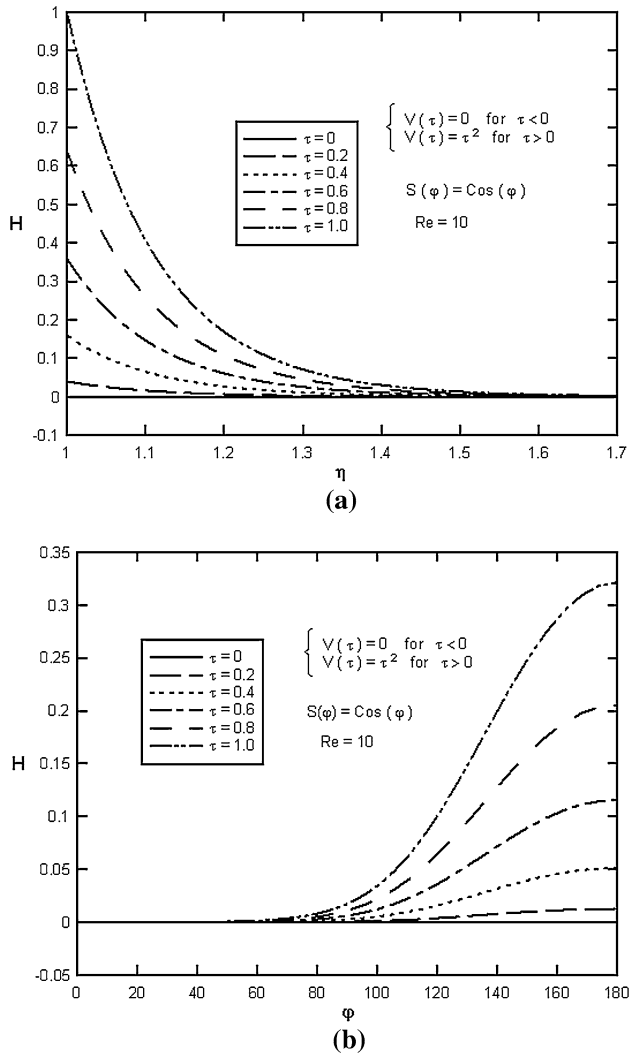

Fig. 4 Sample profiles of $H(\eta,\ \varphi,\ \tau)$ for axial velocity functions $V(\tau) = \tau^2$ in terms of **a** η, **b** φ at Re = 10, $S(\varphi) = Cos(\varphi)$ and for selected values of time steps

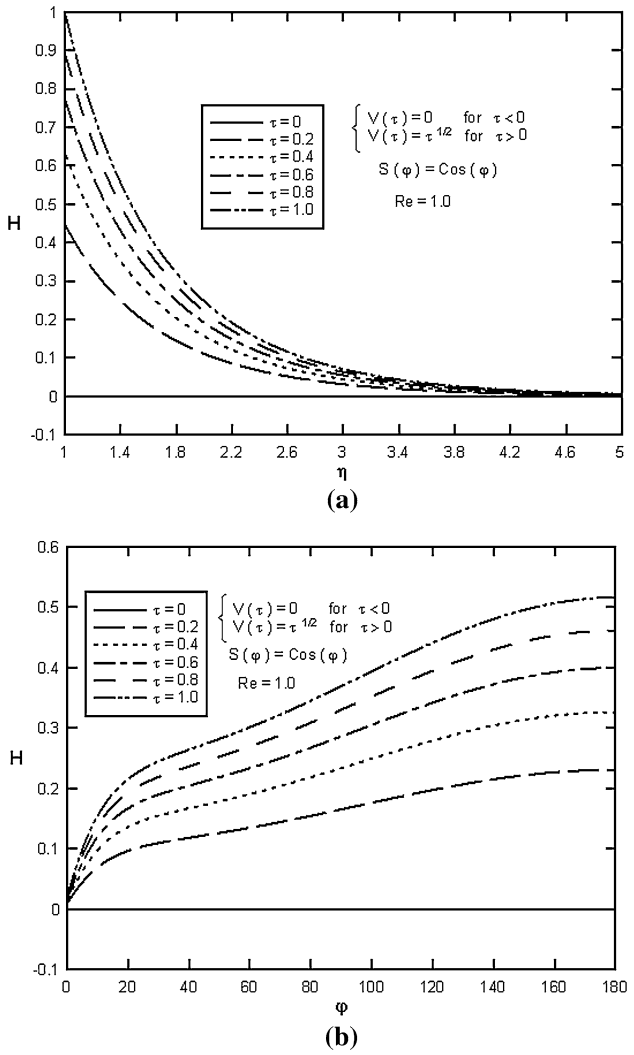

Fig. 5 Sample profiles of $H(\eta,\ \varphi,\ \tau)$ for axial velocity functions $V(\tau) = \tau^{\frac{1}{2}}$ in terms of **a** η, **b** φ at Re = 1.0, $S(\varphi) = Cos(\varphi)$ and for selected values of time steps

$$f(\eta,\ 0,\ \tau) = f(\eta,\ 2\pi,\ \tau),\ \frac{\partial f(\eta,\ 0,\ \tau)}{\partial \varphi} = \frac{\partial f(\eta,\ 2\pi,\ \tau)}{\partial \varphi} \tag{16}$$

In which, $S(\varphi) = U_0(\varphi)/\bar{k}a$ is the transpiration rate function. Note that Equations (11), (12) and (13) are the complete form of Equations (9) and (12), (13) in Ref. [15]. These equations are the same if transpiration rate is constant.

For the sake of brevity, only results for selected values of $S(\varphi) = Cos(\varphi)$, $S(\varphi) = Ln(\varphi)$ are shown in this paper.

To transform the energy equation into a non-dimensional form for the case of defined wall temperature, we introduce

$$\theta(\eta,\ \varphi,\ \tau) = \frac{T(\eta,\ \varphi,\ \tau) - T_\infty}{T_{\mathrm{W}}(\tau) - T_\infty} \tag{17}$$

Making use of Equations (10) and (17), the energy equation, with neglecting the small dissipation terms, may be written as:

$$\eta\theta'' + \theta' + \frac{1}{4\eta}\frac{\partial^2\theta}{\partial\varphi^2} + \mathrm{Re}\cdot\mathrm{Pr}\left(f\theta' - \frac{\partial\theta}{\partial\tau} - \frac{\frac{\partial T_{\mathrm{W}}}{\partial\tau}}{T_{\mathrm{W}} - T_\infty}\theta\right) = 0 \tag{18}$$

With boundary conditions as:

$$\begin{aligned} &\eta = 1: \quad \theta(1,\varphi,\tau) = 1 \\ &\eta \to \infty: \quad \theta(\infty,\varphi,\tau) = 0 \end{aligned} \tag{19}$$

$$\theta(r,\ 0,\ \tau) = \theta(r,\ 2\pi,\ \tau),\ \frac{\partial\theta(r,\ 0,\ \tau)}{\partial\varphi} = \frac{\partial\theta(r,\ 2\pi,\ \tau)}{\partial\varphi} \tag{20}$$

For the case of defined wall heat flux, we introduce

$$\theta(\eta,\ \varphi,\ \tau) = \frac{T(\eta,\ \varphi,\ \tau) - T_\infty}{aq_{\mathrm{W}}(\tau)/2k} \tag{21}$$

Now making use of Equations (10) and (21), the energy equation may be written as:

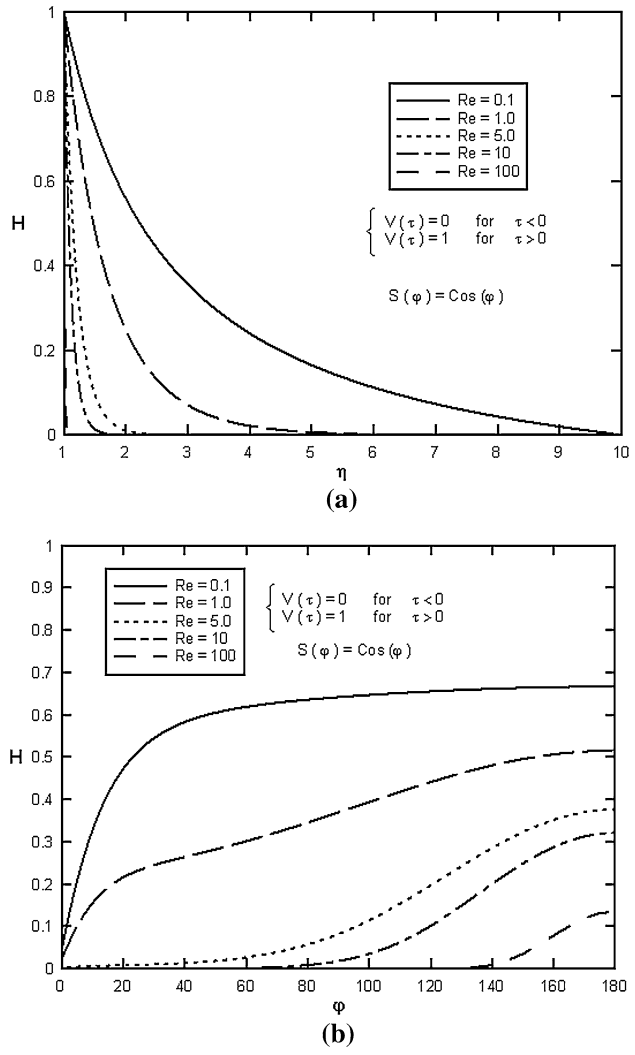

Fig. 6 Sample profiles of $H(\eta,\ \varphi,\ \tau)$ for step-function axial velocity in terms of **a** η, **b** φ at $\tau = 0.1$, $S(\varphi) = Cos(\varphi)$ and for selected values of Reynolds numbers

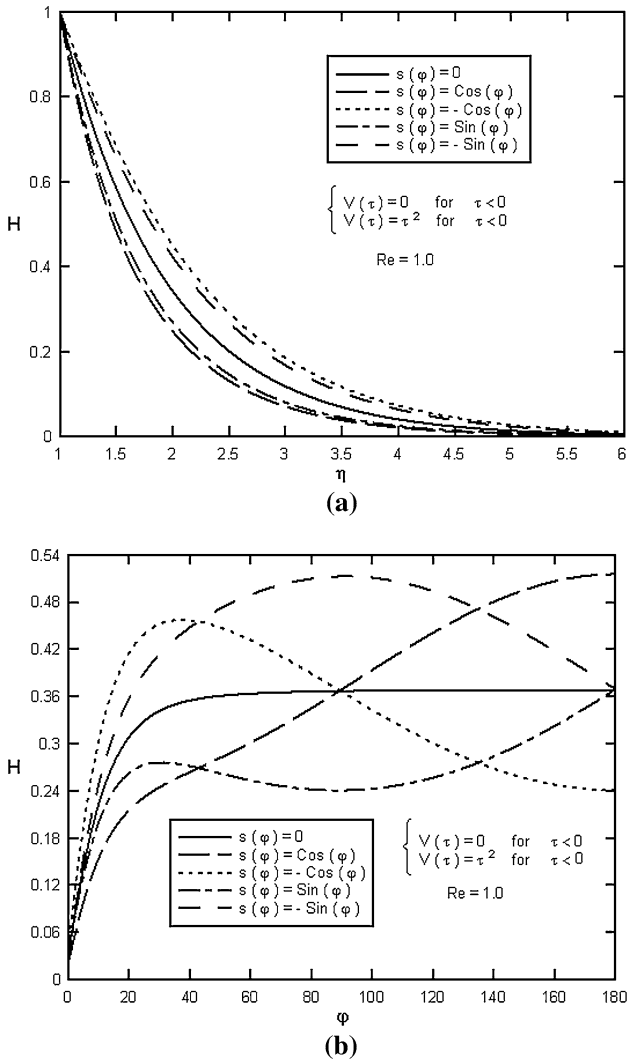

Fig. 7 Sample profiles of $H(\eta,\ \varphi,\ \tau)$ for axial velocity functions $V(\tau) = \tau^2$ in terms of **a** η, **b** φ at Re = 1.0 and for selected values of transpiration rate function

$$\eta\theta'' + \theta' + \frac{1}{4\eta}\frac{\partial^2\theta}{\partial\varphi^2} + \mathrm{Re}\cdot\mathrm{Pr}\left(f\theta' - \frac{\partial\theta}{\partial\tau} - \frac{\frac{\partial q_w}{\partial\tau}}{q_w}\theta\right) = 0 \tag{22}$$

With boundary conditions as:

$$\begin{aligned} \eta = 1: &\quad \theta'(1,\varphi,\tau) = -1 \\ \eta \to \infty: &\quad \theta(\infty,\varphi,\tau) = 0 \end{aligned} \tag{23}$$

$$\theta(r,\ 0,\ \tau) = \theta(r,\ 2\pi,\ \tau),\ \frac{\partial\theta(r,\ 0,\ \tau)}{\partial\varphi} = \frac{\partial\theta(r,\ 2\pi,\ \tau)}{\partial\varphi} \tag{24}$$

Note that Equations (18) and (22) are the complete form of equations (20) in Ref. [15]. These equations are the same if transpiration rate is constant.

Equations (12), (13), (18) and (22), along with boundary conditions (14), (15), (16), (19), (20), (23) and (24), have been solved numerically by an implicit, iterative tri-diagonal finite difference method similar to that discussed by Blottner [29]. To assess the grid independence of the numerical scheme, the distributions of the $H(\eta,\ \varphi,\ \tau)$ function against η on the cylinder were initially tested with different $(\eta,\ \varphi)$ mesh sizes of 51×18, 92×32, 166×58, 299×104 and 538×187 in Fig. 2a. In this set of mesh sizes, as can be seen, the coefficient of 1.8 was used in each test to increase the number of mesh grids in both directions of η and φ. It was found that the variations of the $H(\eta,\ \varphi,\ \tau)$ function distributions on the cylinder were not significant, between $(\eta,\ \varphi)$ and mesh sizes of (166×58), (299×104) and (538×187). Hence, a (299×104) grid in $\eta - \varphi$ directions was applied for the computational domain in the cylinder. Fine, non-uniform grid spacing is used in the η-direction to capture the rapid changes, such as grid

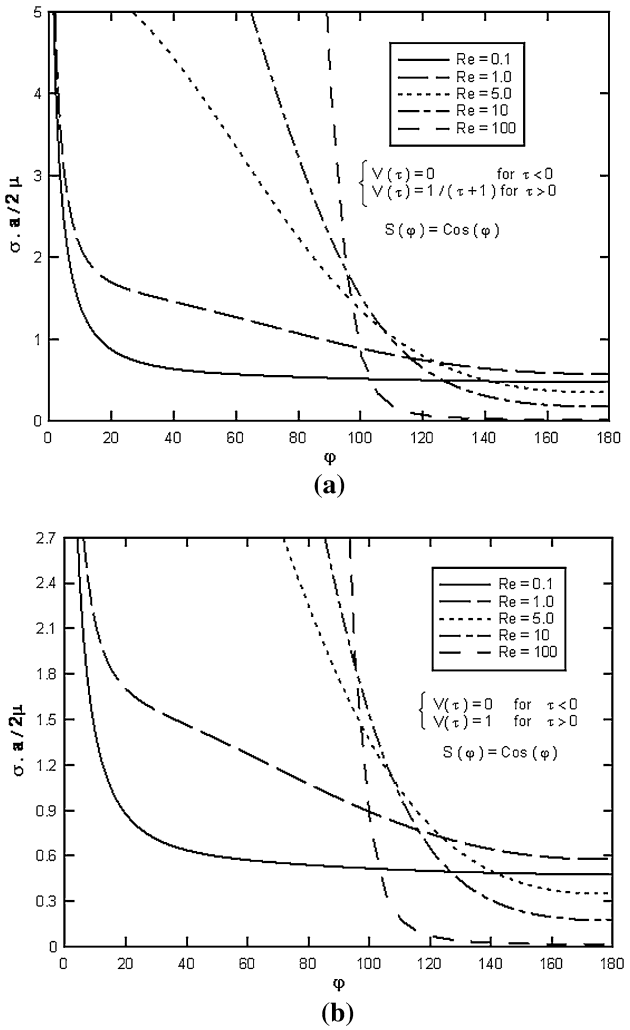

Fig. 8 Sample profiles of $\frac{\sigma \cdot a}{2\mu}$ (shear stress) at $S(\varphi) = Cos(\varphi)$ and for selected values of Reynolds numbers **a** for axial velocity functions $V(\tau) = \frac{1}{1+\tau}$. **b** for step-function axial velocity

lines, being closer packed near the walls. On the other hand, a uniform mesh was implemented in the φ-direction. Figure 2b illustrates a sample of computational meshes used in this investigation.

3 Shear stress

The shear stress at the cylinder surface is calculated from:

$$\sigma = \mu \left[\frac{\partial w}{\partial r}\right]_{r=a} \tag{25}$$

where μ is the fluid viscosity. Using definition (10), the shear stress at the cylinder surface for semi-similar solutions becomes:

$$\sigma = \mu \frac{2}{a}\left[2\bar{k}zf''(1,\ \varphi,\ \tau) + H'(1,\ \varphi,\ \tau)\right] \tag{26}$$

Results for ${}^{\sigma a}/_{2\mu}$ against φ for different values of Reynolds numbers and transpiration rate function in $z = 0$ are presented later.

4 Heat transfer coefficient

The local heat transfer coefficient and rate of heat transfer for defined wall temperature case are given by:

$$h = \frac{q_w}{T_w - T_\infty} = \frac{-k\left(\frac{\partial T}{\partial r}\right)_{r=a}}{T_w - T_\infty} = -\frac{2k}{a}\frac{\partial\theta(1,\ \varphi,\ \tau)}{\partial\eta} \tag{27}$$

where

$$q_w = -\frac{2k}{a}\frac{\partial\theta(1,\ \varphi,\ \tau)}{\partial\eta}(T_w - T_\infty) \tag{28}$$

In terms of Nusselt number:

$$Nu = \frac{ha}{2k} = -\theta'(1,\ \varphi,\ \tau) \tag{29}$$

And for defined wall heat flux case

$$h = \frac{q_w}{T_w - T_\infty} = \frac{-k\left(\frac{\partial T}{\partial r}\right)_{r=a}}{T_w - T_\infty} = \frac{2k}{a}\frac{1}{\theta(1,\ \varphi,\ \tau)} \tag{30}$$

where

$$q_w = \frac{2k}{a}\frac{1}{\theta(1,\ \varphi,\ \tau)}(T_w - T_\infty) \tag{31}$$

In terms of Nusselt number:

$$Nu = \frac{ha}{2k} = \frac{1}{\theta(1,\ \varphi,\ \tau)} \tag{32}$$

5 Presentation of results

In this section, solution of semi-similar Equations (12), (13), (18) and (22) along with surface shear stresses for different function of axial velocity prescribed values of surface temperature or surface heat flux and selected values of Reynolds and Prandtl numbers and transpiration rate function are presented. For the sake of brevity, only results for selected values of $S(\varphi) = Cos(\varphi)$, $S(\varphi) = Ln(\varphi)$ are shown in this paper.

a) $S(\varphi) = Cos(\varphi)$

Figures 3, 4 and 5 present the semi-similar solution for different forms of time-dependent axial velocity in which the function $H(\eta, \varphi, \tau)$ is shown in terms of η and φ for different non-dimensional time values and Reynolds numbers for transpiration rate function $S(\varphi) = Cos(\varphi)$. The solution of ramp function with time steps at Re = 10 and

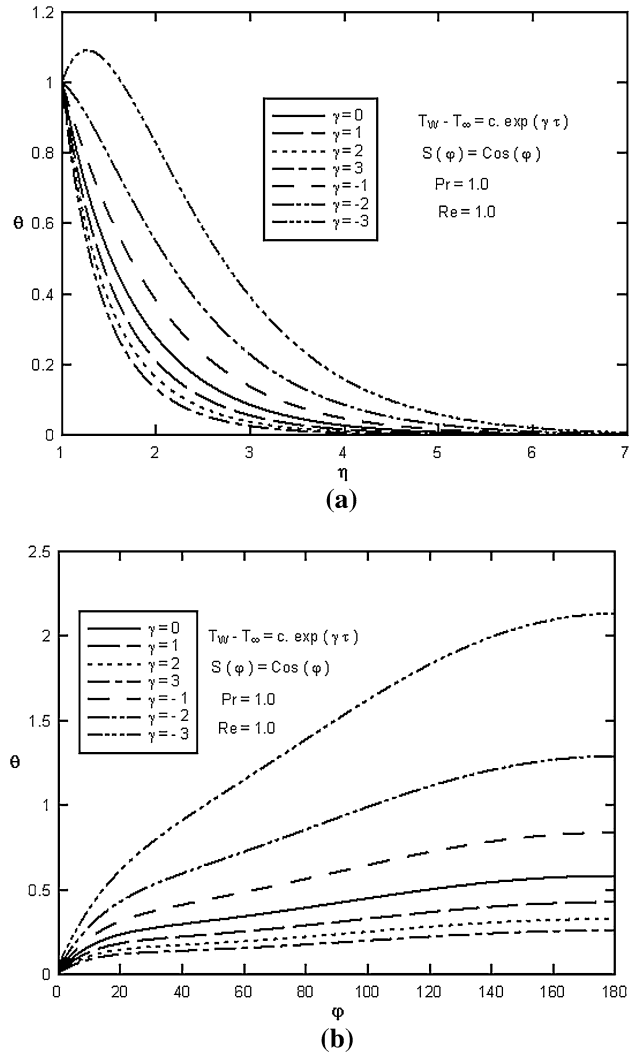

Fig. 9 Sample profiles of $\theta(\eta, \varphi, \tau)$ for wall temperature, varying exponentially with time in Re = 1.0, Pr = 1.0 and $S(\varphi) = Cos(\varphi)$ in terms of a η, b φ

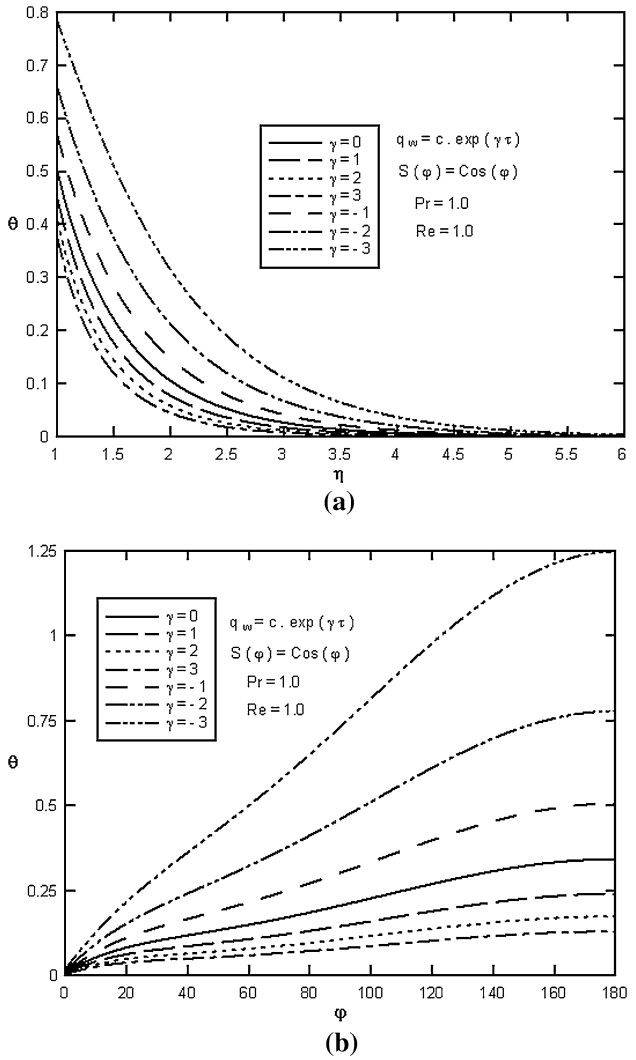

Fig. 10 Sample profiles of $\theta(\eta, \varphi, \tau)$ for wall heat flux, varying exponentially with time in Re = 1.0, Pr = 1.0 and $S(\varphi) = Cos(\varphi)$ in terms of **a** η, **b** φ

$S(\varphi) = Cos(\varphi)$ is shown in Fig. 3, the solution of nonlinear function, the axial velocity of the cylinder at $\tau \langle 0$ is equal to zero and at $\tau \geq 0$ its value becomes $V(\tau) = \tau^2$ suddenly, with time steps at Re = 10 and $S(\varphi) = Cos(\varphi)$ is shown in Fig. 4, the solution of nonlinear function, the axial velocity of the cylinder at $\tau \langle 0$ is equal to zero and at $\tau \geq 0$ its value becomes $V(\tau) = \tau^{\frac{1}{2}}$ suddenly, with time steps at Re = 10 and $S(\varphi) = Cos(\varphi)$ is shown in Fig. 5. In all these forms which as time passes and along with increasing velocity, the thickness of the boundary layer increases.

Sample profiles of the $H(\eta, \varphi, \tau)$ function against η and φ for selected time-dependent axial velocity and for selected values of Reynolds numbers are presented in Fig. 6. As Reynolds number increases, the depth of diffusion of the fluid velocity field in radial and angular direction increases. Effects of transpiration rate function on $H(\eta, \varphi, \tau)$ function against η and φ for selected time-dependent axial velocity and for selected value of Reynolds number Re = 1.0 are shown in Fig. 7. For $S(\varphi) = 0$, axisymmetric stagnation-point flow, the results of Saleh [15] are extracted. In this figure, negative $S(\varphi)$ is blowing rate and positive $S(\varphi)$ is the suction rate. It is evident from this figure that, as transpiration rate function increases, the $H(\eta, \varphi, \tau)$ function increases and if $S(\varphi)$ decreases, the $H(\eta, \varphi, \tau)$ function decreases. It is interesting to note that, as $S(\varphi)$ increases, the depth of diffusion of the fluid velocity field in radial and angular direction increases.

Sample profiles of surface shear stress against φ for Re = 1.0, Pr = 1.0 and $S(\varphi) = Cos(\varphi)$ are shown in Fig. 8, for different axial velocity functions and for selected values of Reynolds numbers. The increase of Reynolds number

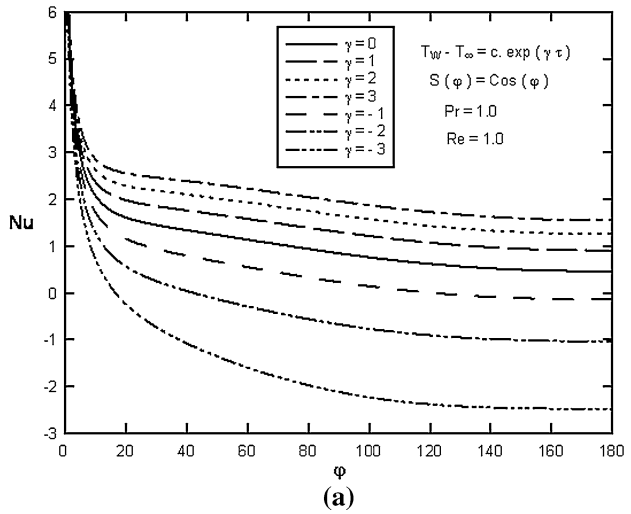

Fig. 11 Sample profiles of *Nu* (Nusselt number) for Re = 1.0, Pr = 1.0 and $S(\varphi) = Cos(\varphi)$. **a** for wall temperature, varying exponentially with time. **b** for wall heat flux, varying exponentially with time $S(\varphi) = Ln(\varphi)$

increases the wall shear stress in φ direction and, on the other hand, causes that the value of fluid velocity in this direction approaches its value in inviscid flow, rapidly. In fact the increase of Reynolds number decreases the thickness of the boundary layer.

Sample profiles of the $\theta(\eta, \varphi, \tau)$ function for wall temperature and wall heat flux, both varying exponentially with time at Re = 1.0, Pr = 1.0 and $S(\varphi) = Cos(\varphi)$, are presented in Figs. 9 and 10, for selected values of γ. From Fig. 9, it is seen that for $\gamma \rangle 0$ the absolute value of the initial slope of the temperature increases with increasing values of γ, and considering Eq. (27), in fact the coefficient of heat transfer increases. Also, from Fig. 10, the temperature on the surface of the cylinder decreases with increasing values of γ, and considering Eq. (30), in fact the coefficient of heat

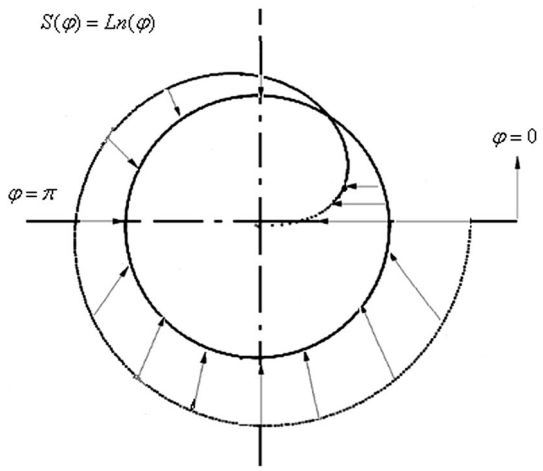

Fig. 12 Schematic diagram of the transpiration function. $S(\varphi) = Ln(\varphi)$

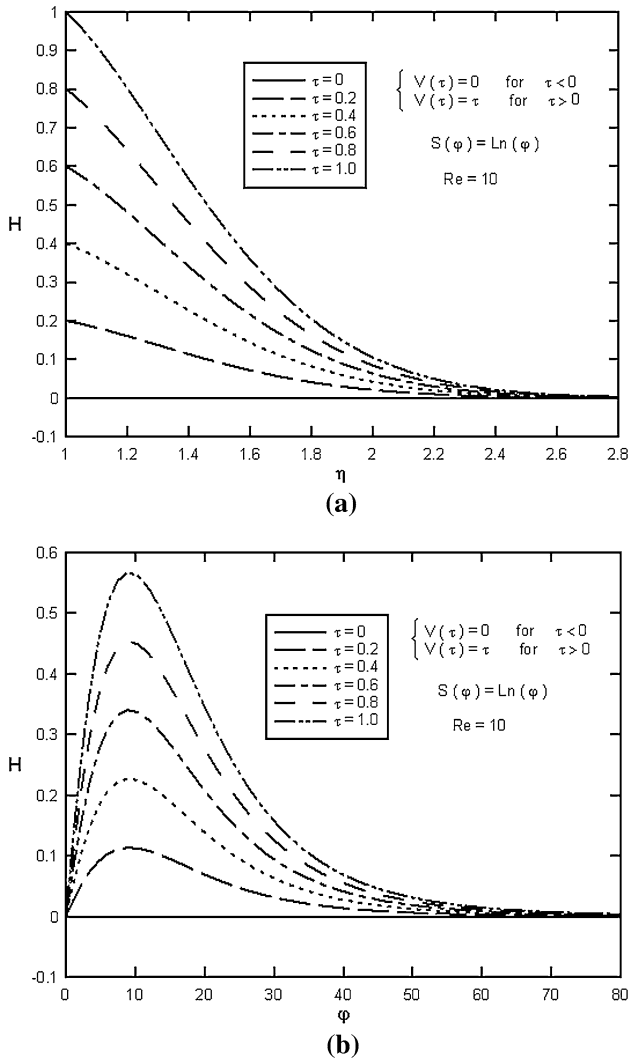

Fig. 13 Sample profiles of $H(\eta, \varphi, \tau)$ for axial velocity functions $V(\tau) = \tau$ in terms of **a** η, **b** φ at Re = 10, $S(\varphi) = Ln(\varphi)$ and for selected values of time steps

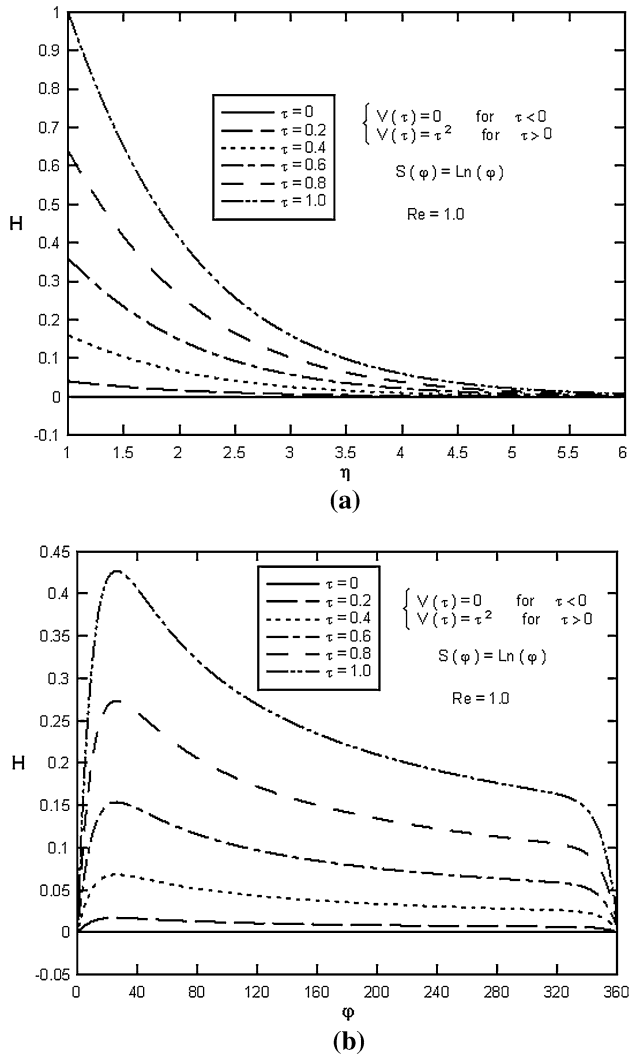

Fig. 14 Sample profiles of $H(\eta, \varphi, \tau)$ for axial velocity functions $V(\tau) = \tau^2$ in terms of **a** η, **b** φ at Re = 10, $S(\varphi) = Ln(\varphi)$ and for selected values of time steps

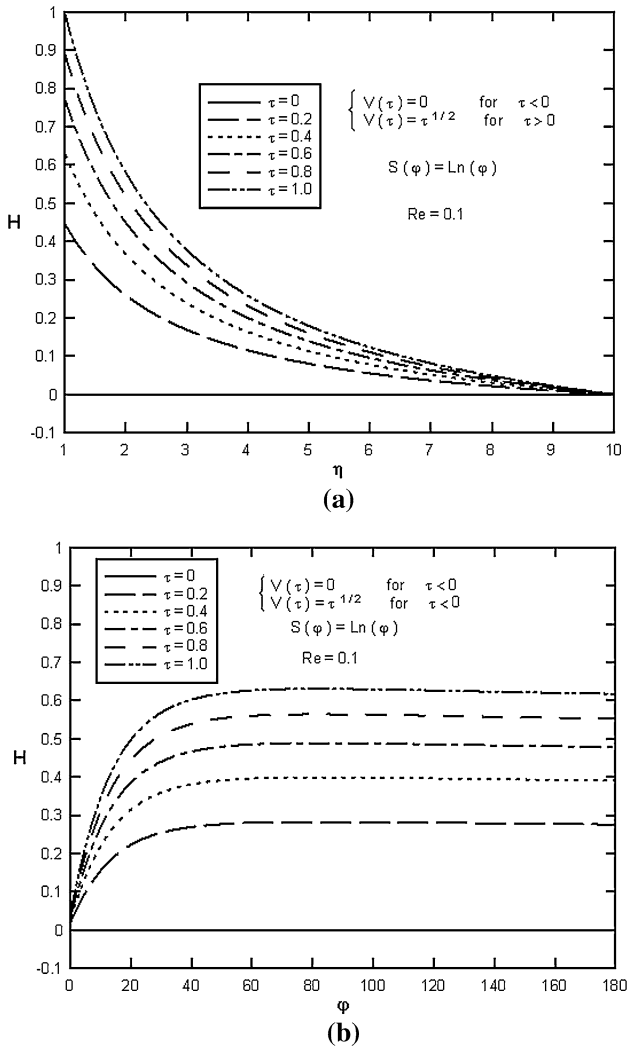

Fig. 15 Sample profiles of $H(\eta, \varphi, \tau)$ for axial velocity functions $V(\tau) = \tau^{\frac{1}{2}}$ in terms of **a** η, **b** φ at Re = 1.0, $S(\varphi) = Ln(\varphi)$ and for selected values of time steps

transfer increases. Further, as transpiration rate function increases, the effect of variation of γ fades away. Therefore, it can be concluded that suction provides a means for cooling the surface, and blowing provides a means for heating the surface of the cylinder. This is rather obvious since in former case there is more contact of free stream fluid with the cylinder and in the latter case relatively less contact of free stream fluid with cylinder takes place. Note that in Figs. 9 and 10 for $\gamma \langle 0$ and any particular value of transpiration rate function, as the absolute value of γ increases beyond certain value, the fluid in the vicinity of the cylinder is not cooled as fast as the cylinder wall and, therefore, the flow temperature here is greater than the wall temperature. It is interesting to note that at any transpiration rate function there is a certain value of negative γ for which the slope of the temperature on the surface becomes zero and, therefore, there is no heat transfer. This is to be expected since the natural diffusion of temperature difference in the fluid and the reduction of the temperature of the cylinder surface are happening in the same manner, then no heat is transferred between the fluid and the cylinder. From both these figures and for $S(\varphi) = S =$ constant and $\theta = \theta(\eta, \tau)$, the results of Saleh and Rahimi [15] are obtained (Fig. 11).

Sample profiles of the Nusselt number (local heat transfer coefficient) for wall temperature and wall heat flux, both varying exponentially with time at Re = 1.0, Pr = 1.0 and $S(\varphi) = Cos(\varphi)$, are shown in Fig. 10, for selected values of γ. Here, the Nusselt number increases with increases in γ (Fig. 12).

Figures 13, 14 and 15 present the semi-similar solution for different forms of time-dependent axial velocity in which the function $H(\eta, \varphi, \tau)$ is shown in terms of η

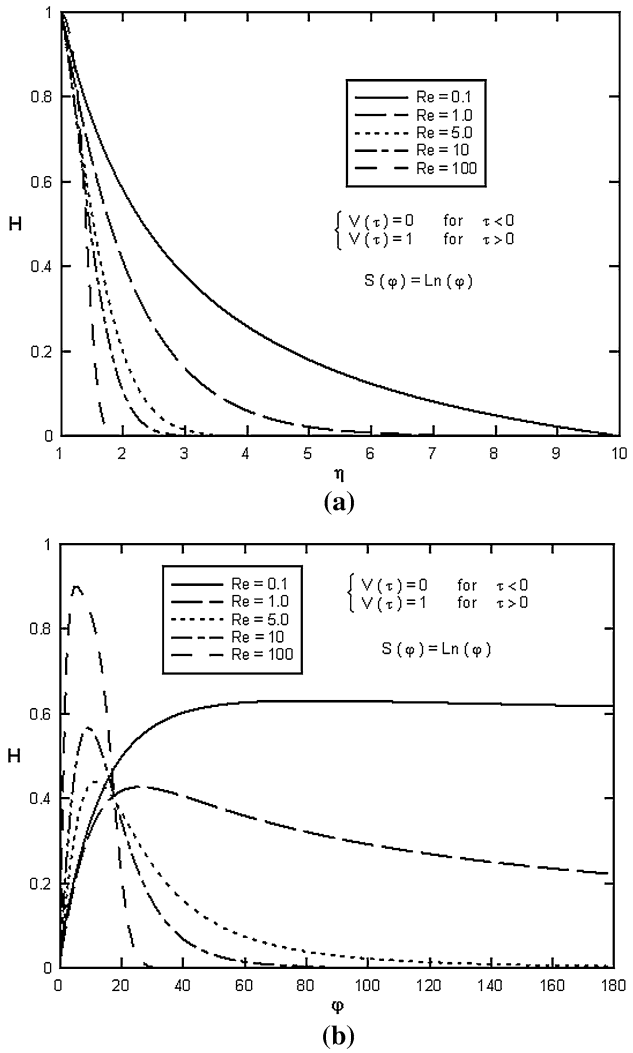

Fig. 16 Sample profiles of $H(\eta,\ \varphi,\ \tau)$ for step-function axial velocity in terms of **a** η, **b** φ at $\tau = 0.1$, $S(\varphi) = Ln(\varphi)$ and for selected values of Reynolds numbers

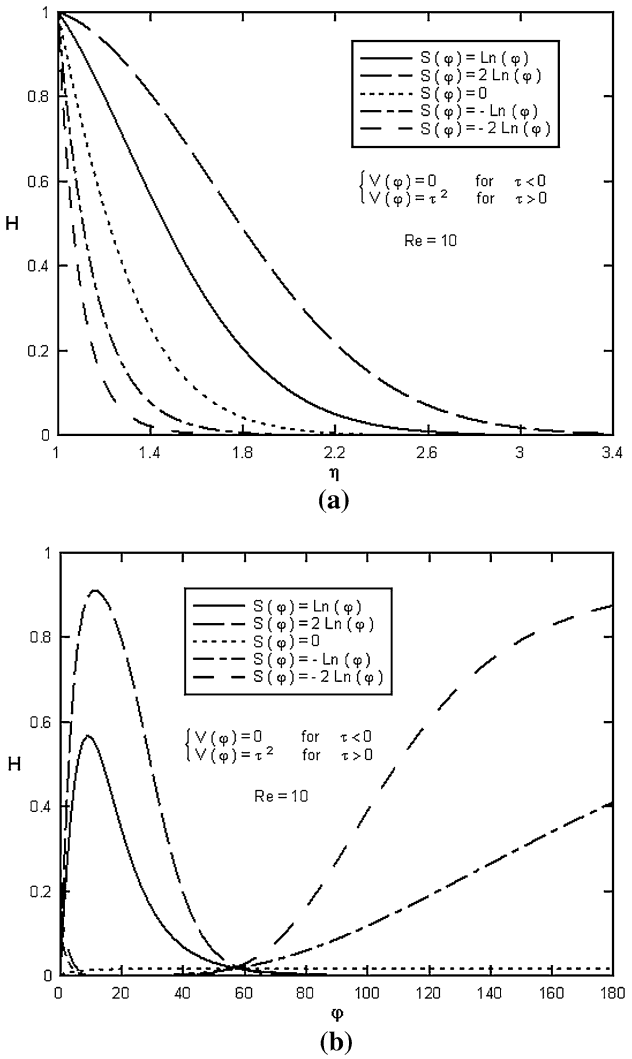

Fig. 17 Sample profiles of $H(\eta,\ \varphi,\ \tau)$ for axial velocity functions $V(\tau) = \tau^2$ in terms of **a** η, **b** φ at Re = 1.0, $S(\varphi) = Ln(\varphi)$ and for selected values of transpiration rate function

and φ for different non-dimensional time values and Reynolds numbers for transpiration rate function $S(\varphi) = Ln(\varphi)$. The solution of ramp function with time steps at Re = 10 and $S(\varphi) = Ln(\varphi)$ is shown in Fig. 13, the solution of nonlinear function, the axial velocity of the cylinder at $\tau \langle 0$ is equal to zero and at $\tau \geq 0$ its value becomes $V(\tau) = \tau^2$ suddenly, with time steps at Re = 10 and $S(\varphi) = Ln(\varphi)$ is shown in Fig. 14, the solution of nonlinear function, the axial velocity of the cylinder at $\tau \langle 0$ is equal to zero and at $\tau \geq 0$ its value becomes $V(\tau) = \tau^{\frac{1}{2}}$ suddenly, with time steps at Re = 10 and $S(\varphi) = Ln(\varphi)$ is shown in Fig. 15. In all these forms which as time passes and along with increasing velocity, the thickness of the boundary layer inc reases.

Sample profiles of the $H(\eta, \varphi, \tau)$ function against η and φ for selected time-dependent axial velocity and for selected values of Reynolds numbers are presented in Fig. 16. As Reynolds number increases, the depth of diffusion of the fluid velocity field in radial and angular direction increases. Effects of transpiration rate function on $H(\eta, \varphi, \tau)$ function against η and φ for selected time-dependent axial velocity and for selected value of Reynolds number Re = 1.0 are shown in Fig. 17. For $S(\varphi) = 0$, axisymmetric stagnation-point flow, the results of Saleh [15] are extracted. In this figure negative, $S(\varphi)$ is blowing rate and positive $S(\varphi)$ is the suction rate. It is evident from this figure that, as transpiration rate function increases, the $H(\eta, \varphi, \tau)$ function increases and if $S(\varphi)$ decreases, the $H(\eta, \varphi, \tau)$ function decreases. It is interesting to note that, as $S(\varphi)$ increases, the depth of diffusion of the fluid velocity field in radial and angular direction increases.

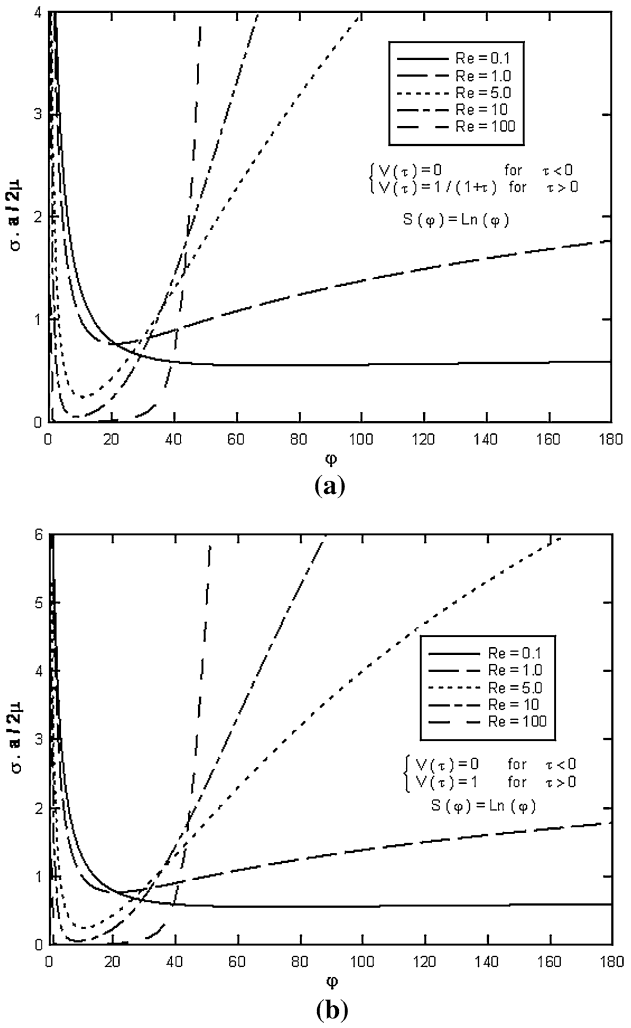

Fig. 18 Sample profiles of $\frac{\sigma \cdot a}{2\mu}$ (shear stress) at $S(\varphi) = Ln(\varphi)$ and for selected values of Reynolds numbers **a** for axial velocity functions $V(\tau) = \frac{1}{1+\tau}$ **b** for step-function axial velocity

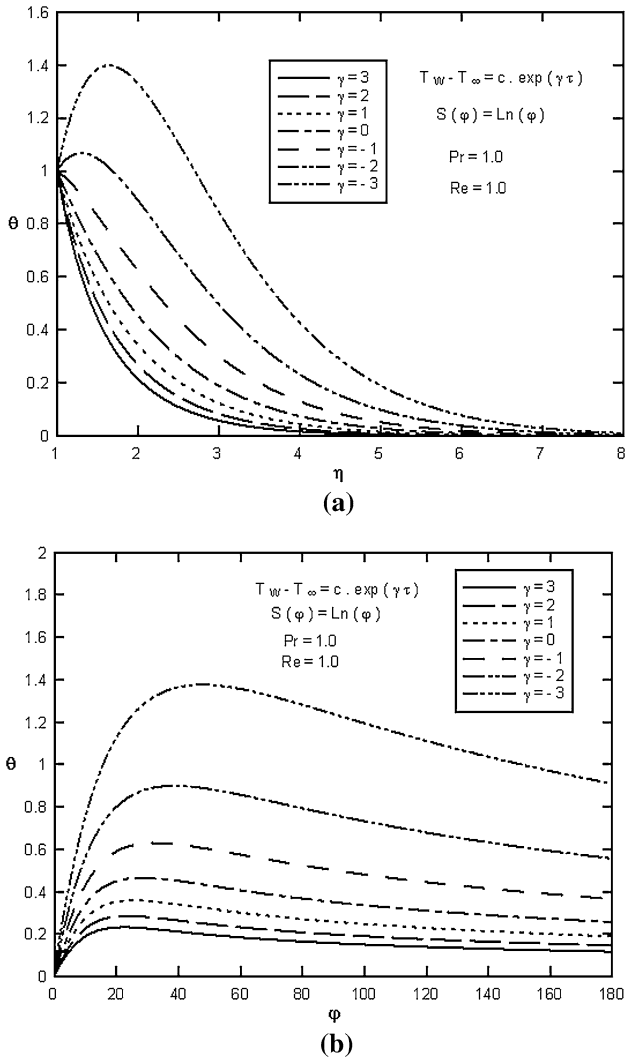

Fig. 19 Sample profiles of $\theta(\eta, \varphi, \tau)$ for wall temperature, varying exponentially with time in Re = 1.0, Pr = 1.0 and $S(\varphi) = Ln(\varphi)$ in terms of **a** η, **b** φ

Sample profiles of surface shear stress against φ for Re = 1.0, Pr = 1.0 and $S(\varphi) = Ln(\varphi)$ are shown in Fig. 18, for different axial velocity functions and for selected values of Reynolds numbers. The increase of Reynolds number increases the wall shear stress in φ direction and, on the other hand, causes that the value of fluid velocity in this direction approaches its value in inviscid flow, rapidly. In fact the increase of Reynolds number decreases the thickness of the boundary layer.

Sample profiles of the $\theta(\eta, \varphi, \tau)$ function for wall temperature and wall heat flux, both varying exponentially with time at Re = 1.0, Pr = 1.0 and $S(\varphi) = Ln(\varphi)$, are presented in Figs. 19 and 20, for selected values of γ. From Fig. 18, it is seen that for $\gamma \rangle 0$ the absolute value of the initial slope of the temperature increases with increasing values of γ, and considering Eq. (27), in fact the coefficient of heat transfer increases. Also, from Fig. 20, the temperature on the surface of the cylinder decreases with increasing values of γ, and considering Eq. (30), in fact the coefficient of heat transfer increases. Further, as transpiration rate function increases, the effect of variation of γ fades away. Therefore, it can be concluded that suction provides a means for cooling the surface, and blowing provides a means for heating the surface of the cylinder. This is rather obvious since in former case there is more contact of free stream fluid with the cylinder and in the latter case relatively less contact of free stream fluid with cylinder takes place. Note that in Figs. 19 and 20 for $\gamma \langle 0$ and any particular value of transpiration rate function, as the absolute value of γ increases beyond certain value, the fluid in the vicinity of the cylinder is not cooled as fast as the cylinder wall and, therefore, the flow temperature here is greater than the wall temperature. It is interesting to note that

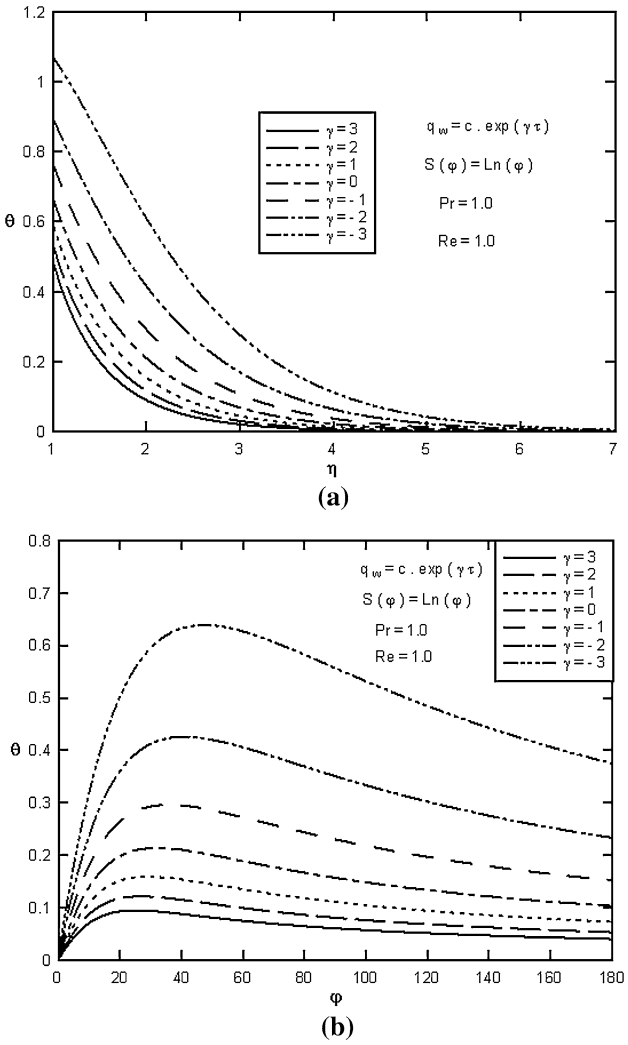

Fig. 20 Sample profiles of $\theta(\eta, \varphi, \tau)$ for wall heat flux, varying exponentially with time in Re = 1.0, Pr = 1.0 and $S(\varphi) = Ln(\varphi)$ in terms of **a** η, **b** φ

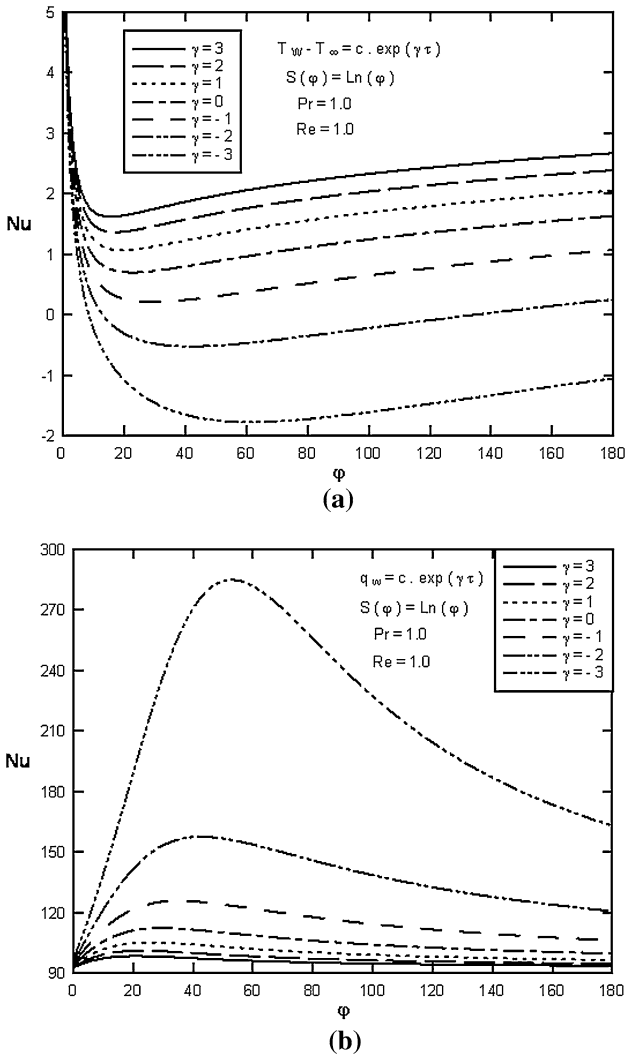

Fig. 21 Sample profiles of *Nu* (Nusselt number) for Re = 1.0, Pr = 1.0 and $S(\varphi) = Ln(\varphi)$. **a** For wall temperature, varying exponentially with time. **b** For wall heat flux, varying exponentially with time

at any transpiration rate function there is a certain value of negative γ for which the slope of the temperature on the surface becomes zero and, therefore, there is no heat transfer. This is to be expected since the natural diffusion of temperature difference in the fluid and the reduction of the temperature of the cylinder surface are happening in the same manner, then no heat is transferred between the fluid and the cylinder. From both these figures and for $S(\varphi) = S =$ constant and $\theta = \theta(\eta, \tau)$, the results of Saleh and Rahimi [15] are obtained.

Sample profiles of the Nusselt number (local heat transfer coefficient) for wall temperature and wall heat flux, both varying exponentially with time at Re = 1.0, Pr = 1.0 and $S(\varphi) = Ln(\varphi)$, are shown in Fig. 21, for selected values of γ. Here, the Nusselt number increases with increases in γ.

6 Conclusions

The unsteady viscous flow and heat transfer in the vicinity of an unaxisymmetric stagnation-point flow of an infinite moving cylinder with time-dependent axial velocity and non-uniform normal transpiration $U_0(\varphi)$ are investigated. A reduction of the Navier–Stokes and energy equations has been obtained by use of appropriate similarity transformations. The semi-similar solution of the Navier–Stokes equations and energy equation has been obtained numerically using an implicit finite-difference scheme when the axial velocity of the cylinder and its wall temperature or its wall heat flux vary as specified time-dependent functions. In particular, the cylinder may move with different velocity patterns. These solutions are presented for special

cases when the time-dependent axial velocity of the cylinder is a step function, a ramp, and a non-linear function. All the solutions above have been presented for Reynolds numbers ranging from 0.01 to 100 for different values of Prandtl number and for selected values of transpiration rate function. For all transpiration rate functions with increase in Reynolds numbers, both components of the velocity field increase and for all transpiration rate function with increase in γ the temperature field decreases. Dimensionless shear stresses corresponding to all the cases increase with the increase of Reynolds number and transpiration rate function. The local coefficient of heat transfer (Nusselt number) increases with the increasing transpiration rate function and γ. Also increase of suction rate can be used as a means of cooling the surface and increase of blowing rate can be used as a means of heating the surface. For the case of axisymmetric stagnation-point flow, $f = f(\eta)$, $H = H(\eta)$, $f' = f'(\eta)$ and $S(\varphi) = 0$ or $\partial^2 f/\partial\phi^2 = 0$, $\partial^2 f'/\partial\phi^2 = 0$, $\partial^2 H/\partial\phi^2 = 0$, $\partial^2\theta/\partial\phi^2 = 0$ and similarity variables and component of velocity by Wang [5], as well as energy equation by Gorla [7] and Saleh and Rahimi [15] are reached.

References

1. Hiemenz K (1911) Die Grenzschicht an einem in den gleichförmingen Flüssigkeitsstrom eingetauchten geraden Kreiszylinder. Dinglers Polytechnisches Journal 326:321–410
2. Homann FZ (1936) Der Einfluss Grosser Zahighkeit bei der Strmung um den Zylinder und um die Kugel. Zeitschrift für angewandte Mathematik und Mechanik 16:153–164. doi:10.1002/zamm.19360160304
3. Howarth L (1951) The boundary layer in three-dimensional flow. Part 2. The flow near stagnation point. Philos Mag 42(7):1433–1440
4. Davey A (1961) Boundary-layer flow at a saddle point of attachment. J Fluid Mech 10(4):593–610. doi:10.1017/S0022112061000391
5. Wang CY (1974) Axisymmetric stagnation flow on a cylinder. Q Appl Math 32:207–213
6. Wang CY (1973) Axisymmetric stagnation flow towards a moving plate. Am Inst Chem Eng J 19(5):1080–1082. doi:10.1002/aic.690190540
7. Gorla RSR (1976) Heat transfer in an axisymmetric stagnation flow on a cylinder. Appl Sci Res 32(5):541–553. doi:10.1007/BF00385923
8. Gorla RSR (1977) Unsteady laminar axisymmetric stagnation flow over a circular cylinder. Dev Mech 9:286–288
9. Gorla RSR (1978) Non-similar axisymmetric stagnation flow on a moving cylinder. Int J Eng Sci 16(6):392–400
10. Gorla RSR (1978) Transient response behavior of an axisymmetric stagnation flow on a circular cylinder due to time-dependent free stream velocity. Lett Appl Eng Sci Int J 16(7):493–502. doi:10.1016/0020-7225(78)90082-4
11. Gorla RSR (1979) Unsteady viscous flow in the vicinity of an axisymmetric stagnation-point on a cylinder. Int J Eng Sci 17(1):87–93. doi:10.1016/0020-7225(79)90009-0
12. Cunning GM, Davis AMJ, Weidman PD (1998) Radial stagnation flow on a rotating cylinder with uniform transpiration. J Eng Math 33(2):113–128. doi:10.1023/A:1004243728777
13. Grosch CE, Salwen H (1982) Oscillating stagnation point flow. Proc R Soc Lond Ser A Math Phys Sci 384(786):175–190
14. Takhar HS, Chamkha AJ, Nath J (1999) Unsteady axisymmetric stagnation-point flow of a viscous fluid on a cylinder. Int J Eng Sci 37(15):1943–1957. doi:10.1016/S0020-7225(99)00009-9
15. Saleh R, Rahimi AB (2004) Axisymmetric stagnation-point flow and heat transfer of a viscous fluid on a moving cylinder with time-dependent axial velocity and uniform transpiration. J Fluid Eng 126(6):997–1005. doi:10.1115/1.1845556
16. Rahimi AB, Saleh R (2007) Axisymmetric stagnation-point flow and heat transfer of a viscous fluid on a rotating cylinder with time-dependent angular velocity and uniform transpiration. J Fluid Eng 129(1):107–115
17. Rahimi AB, Saleh R (2008) Similarity solution of unaxisymmetric heat transfer in stagnation-point flow on a cylinder with simultaneous axial and rotational movements. J Heat Transf 130(5):054502-1–054502-5
18. Abbasi AS, Rahimi AB (2009) Non-axisymmetric three-dimensional stagnation-point flow and heat transfer on a flat plate. J Fluid Eng 131(7):074501.1–074501.5
19. Abbasi AS, Rahimi AB (2009) Three-dimensional stagnation-point flow and heat transfer on a flat plate with transpiration. J Thermophys Heat Transf 23(3):513–521. doi:10.2514/1.41529
20. Abbasi AS, Rahimi AB, Niazman H (2011) Exact solution of three-dimensional unsteady stagnation flow on a heated plate. J Thermophy Heat Transf 25(1):55–58. doi:10.2514/1.48702
21. Abbasi AS, Rahimi AB (2012) Investigation of two-dimensional stagnation-point flow and heat transfer impinging on a flat plate. J Heat Transf 134:024501-1
22. Subhashini SV, Nath G (1999) Unsteady compressible flow in the stagnation region of two-dimensional and axisymmetric bodies. Acta Mechanica 134(3–4):135–145. doi:10.1007/BF01312652
23. Kumari M, Nath G (1980) Unsteady compressible 3-dimensional boundary layer flow near an axisymmetric stagnation point with mass transfer. Int J Eng Sci 18(12):1285–1300. doi:10.1016/0020-7225(80)90120-2
24. Kumari M, Nath G (1981) Self-similar solution of unsteady compressible three-dimensional stagnation-point boundary layers. J Appl Math Phys 32(3)
25. Katz A (1972) Transformations of the compressible boundary layer equations. SIAM J Appl Math 22(4)
26. Afzal N, Ahmad S (1975) Effect of transpiration and injection on self-similar solutions of second-order boundary layer equations. Int J Heat Mass Transf 18(5):607–614. doi:10.1016/0017-9310(75)90272-0
27. Libby PA (1967) Heat and mass transfer at a general three-dimensional stagnation point. AIAA J 5(3):507–517. doi:10.2514/3.4008
28. Gersten K, Papenfuss HD, Gross JF (1978) Influence of the Prandtl Number on second-order heat transfer due to surface curvature at a three-dimensional stagnation point. Int J Heat Mass Transf 21(3):275–284. doi:10.1016/0017-9310(78)90120-5
29. Blottner FG (1970) Finite-difference methods of solution of the boundary layer equations. AIAA J 8:193–205